Asia Mathematika
Volume: 5 Issue: 2 , (2021) Pages: 8 – 19
Available online at **www.asiamath.org**

Soret-Dufour effect and higher-order chemical reaction on MHD Casson fluid flow past over a vertical plate with heat source/sink

A.K. Shukla[1*] **and Yogendra Kumar Dwivedi**[2]
[1]Department of mathematics, RSKD PG College Jaunpur, India 222001, Jaunpur, India. Orchid iD: 0000-0002-7049-6780
[2]Department of mathematics, RSKD PG College Jaunpur, India 222001, Jaunpur, India. Orchid iD: 0000-0002-5863-6947

Received: 14 Apr 2021 • **Accepted:** 17 May 2021 • **Published Online:** 25 Aug 2021

Abstract: The objective of this paper is to introduce the effect of Soret-Dufour, a higher-order chemical reaction on MHD Casson fluid with a heat source/sink over a vertical plate embedded in a porous medium. The observation reveals different parts of the flow of Casson fluid, heat, and mass transfer. Crank-Nicolson finite difference method utilized for solving Non-dimensional governing partial differential equations. Computations are executed graphically to analyze the change of velocity, temperature, and concentration as well as Skin-friction, Nusselt number, and Sherwood number for different values of parameters Dufour number $Du = 0.2$, Chemical reaction parameter $Kr = 1.2$, heat source/sink parameter $Q = 2$, Schmidt number $Sc = 0.6$, Soret number $Sr = 1.5$, order of chemical reaction $n = 2$, radiation parameter $R = 2.2$, magnetic parameter $M = 4.8$, Casson parameter $\beta = 0.4$, $t = 0.2$, $Gr = 4$, $Gm = 7$, $K = 1.5$ and $Pr = 0.7$.

Key words: Soret effect, Dufour effect, order of chemical reaction, heat equation, mass equation, heat source and sink, Casson fluid

1. Introduction

An investigation on non-Newtonian fluid flow past a vertical plate has great attention for a long time because there is a large number of applications in Aerodynamics, metallurgical process, glass blowing, manufacturing of rubber, paints, drilling muds, etc. And for different causes, the employment of MHD in such type of flow problems is also developing interest. Shawa and Mahantha[1] investigated the boundary layer movement of a 3D Casson fluid in presence of suction past an exponentially expanding plate. Hayat et al.[2] discussed the starting impacts of magnetic field and the heat sink(source) on unsteady convective heat and mass transfer over a porous plate. Eid et al.[3] analyzed the influence of magnetic parameter on two-phase nanofluid over a porous stretching plate.

Islam et al.[4] studied unsteady Casson fluid flow with heat transfer past over a stretching plate. Sandeep et al.[5] investigated MHD electrically conducting the flow of a micropolar fluid over a frozen surface. Shehzad et al.[6] have been given interpretation of radiation and Lorentz force on the motion of nanofluid flow past over a stretching sheet. Affy studied, by implementing the spectral relaxation process, the effect of radiation, heat source or sink, and Soret-Dufour effects on the Casson fluid with a stretching plate. Alotaibi et al.[8] introduced the effects of heat source(sink) on MHD flow of Casson nanofluid via a nonlinear stretching plate with viscous dissipation. Kirubhashakar et al.[9] studied the heat effect of MHD Casson fluid in presence of heat transfer over

*Correspondence: ashishshukla1987@gmail.com

the inclined plate. Idowu et al.[10] investigated the Cattaneo Christof heat flux relocation paradox on Casson fluid with MHD and dissipative effect. Bhuvaneswari et al.[11] studied the Dufour and Soret effects on MHD mixed convection of a chemically reacting fluid over a stretching surface in a porous medium with convective boundary condition. MHD mixed convection in a square lid-driven cavity filled with gyrotactic micro-organisms is analysed by Mansour et al.[12].

The aim of the current work is to study higher-order chemical reaction with heat source/sink with Soret-Dufour effects on MHD Casson fluid flow past a porous vertical plate. The solution of governing equations is implemented to transform dimensional partial differential equations to nondimensional partial differential equations. The result is obtained by using.

2. Mathematical Analysis

We have considered the unsteady MHD Casson fluid flow past a vertical plate embedded in a porous medium with the Soret-Dufour effect and higher-order chemical reaction as well as heat source/sink. We have also considered that at starting temperature of the plate is T_w^* and concentration is C_w^*. x^*-direction is along with the plate and y^*-direction is normal to it. The plate is impulsively started with velocity U_0. The induced magnetic field is neglected because transverse applied magnetic field and Reynold's number is small.

The velocity, temperature, and the concentration equations in a Casson nanofluid following above-described conditions are written as

$$\frac{\partial v^*}{\partial y^*} = 0 \Rightarrow v^* = -V_0 \tag{1}$$

$$\begin{aligned}\frac{\partial u^*}{\partial t^*} + v^*\frac{\partial u^*}{\partial y^*} =& \nu\left(1+\frac{1}{\beta}\right)\left(\frac{\partial u^*}{\partial y^{*2}}\right) + g\beta_t(T^*-T_\infty^*) + g\beta_c(C^*-C_\infty^*) \\ &- \frac{\sigma B_0^2 u^*}{\rho} - \frac{\nu u^*}{K^*}\end{aligned} \tag{2}$$

$$\rho c_p\left(\frac{\partial T^*}{\partial t^*} + v^*\frac{\partial T^*}{\partial y^*}\right) = k\frac{\partial^2 T^*}{\partial y^{*2}} - \frac{\partial q_r}{\partial y^*} + \frac{\rho D_m K_T}{c_s}\frac{\partial^2 C^*}{\partial y^{*2}} - Q_0(T^*-T_\infty^*) \tag{3}$$

$$\frac{\partial C^*}{\partial t^*} + v^*\frac{\partial C^*}{\partial y^*} = D_m\frac{\partial^2 C^*}{\partial C^{*2}} + \frac{D_m K_T}{T_m}\frac{\partial^2 T^*}{\partial y^{*2}} - k_r(C^*-C_\infty^*)^n \tag{4}$$

where
intial and boundary conditions are:

$$\begin{aligned} u^* = 0 \quad T^* = T_\infty^* \quad C^* = C_\infty^* \quad \text{for} \quad t^* \le 0 \quad \text{and} \quad \forall\, y \\ u^* = U_0 \quad v^* = -V_0 \quad T^* = T_\infty^* + (T_w^* - T_\infty^*)e^{-Bt^*}, \\ C^* = C_\infty^* + (C_w^* - C_\infty^*)e^{-Bt^*}, \quad \text{for} \quad t^* > 0 \quad \text{and} \quad y^* = 0 \\ u^* = 0 \quad T^* \to T_\infty^* \quad C^* \to C_\infty^* \quad \text{for} \quad y^* \to \infty \end{aligned} \tag{5}$$

where the term T_w^* and C_w^* represent temperature and concentration respectively of plate and B is equivalent to $\frac{v_0^2}{\nu}$.

$k_r(C^* - C^*_\infty)^n$	terms in mass equation for higher order chemical reaction
n	order of chemical reaction
k_r	chemical reaction constant
C^*	concentration
T^*	temperature
T^*_∞	temperature of free stream
C^*_∞	concentration of free stream
β	Casson parameter
β_c	coefficient of volume expansion for mass transfer
β_t	volumetric coefficient of thermal expansion
T_m	mean fluid temperature
q_r	radiative heat along y^*-axis
Q_0	Coefficient of heat source/sink
ν	kinematic viscosity
$\tilde{K}$	coefficient of permeability of porous medium
D_m	molecular diffusivity
k	thermal conductivity of fluid
c_p	specific heat at constant pressure
μ	viscosity
ρ	fluid density
σ	electrical conductivity
g	acceleration due to gravity
K_T	thermal diffusion ratio

Roseland explained the term radiative heat flux approximately as

$$q_r = -\frac{4\sigma_{st}}{3a_m}\frac{\partial T^{*4}}{\partial y^*} \tag{6}$$

where σ_{st} is Stefan Boltzmann constant and a_m is the mean absorption coefficient. In equation (6), term T^{*4} can be expressed linearly, using Taylor's series about T^*_∞ and neglect higher-order term because temperature difference within a flow is very small, so

$$T^{*4} \cong 4T^{*3}_\infty T^* - 3T^{*4}_\infty \tag{7}$$

with the help of equations (6) and (7), we write the equation (3) in this way

$$\begin{aligned}\rho c_p\left(\frac{\partial T^*}{\partial t^*} + v^*\frac{\partial T^*}{\partial y^*}\right) =& k\frac{\partial^2 T^*}{\partial y^{*2}} + \frac{16\sigma_{st}T^{*3}_\infty}{3a_m}\frac{\partial^2 T^*}{\partial y^{*2}} + \frac{\rho D_m K_T}{c_s}\frac{\partial^2 C^*}{\partial y^{*2}} \\ &- Q_0(T^* - T^*_\infty)\end{aligned} \tag{8}$$

Let us introduce the following dimensionless quantities

$$\begin{gathered} Du = \frac{D_m K_T (C_w^* - C_\infty^*)}{c_s c_p \nu (T_w^* - T_\infty^*)},\ Sr = \frac{D_m K_T (T_w^* - T_\infty^*)}{T_m \nu (C_w^* - C_\infty^*)},\ u = \frac{u^*}{U_0},\ t = \frac{t^* V_0^2}{\nu}, \\ Gr = \frac{\nu g \beta_t (T_w^* - T_\infty^*)}{U_0 V_0^2},\ Gm = \frac{\nu g \beta_c (C_w^* - C_\infty^*)}{U_0 V_0^2},\ \theta = \frac{T^* - T_\infty^*}{T_w^* - T_\infty^*}, \\ C = \frac{C^* - C_\infty^*}{C_w^* - C_\infty^*},\ K = \frac{V_0^2 K^*}{\nu^2},\ Pr = \frac{\mu c_p}{k},\ M = \frac{\sigma B_0^2 \nu}{\rho V_0^2},\ R = \frac{4\sigma_{st} T^{*3}_\infty}{a_m k}, \\ Sc = \frac{\nu}{D_m},\ y = \frac{y^* V_0}{\nu},\ K_r = \frac{k_r \nu}{V_0^2},\ Q = \frac{Q_0 \nu}{\rho c_p V_0^2}. \end{gathered} \tag{9}$$

To use non dimensional terms, introduced in equation (9), we get non-dimensional form of governing partial differential equations (2), (8) and (4) respectively:

$$\frac{\partial u}{\partial t} - \frac{\partial u}{\partial y} = \left(1 + \frac{1}{\beta}\right) \frac{\partial^2 u}{\partial y^2} + Gr\,\theta + Gm\,C - \left(M + \frac{1}{K}\right) u \tag{10}$$

$$\frac{\partial \theta}{\partial t} - \frac{\partial \theta}{\partial y} = \frac{1}{Pr} \left(1 + \frac{4R}{3}\right) \frac{\partial^2 \theta}{\partial y^2} + Du \frac{\partial^2 C}{\partial y^2} - Q\theta \tag{11}$$

$$\frac{\partial C}{\partial t} - \frac{\partial C}{\partial y} = \frac{1}{Sc} \frac{\partial^2 C}{\partial y^2} + Sr \frac{\partial^2 \theta}{\partial y^2} - K_r C^n \tag{12}$$

with initial and boundary conditions

$$\begin{gathered} u = 0 \quad \theta = 0 \quad C = 0 \quad \text{for} \quad t \le 0 \quad \text{and} \quad \forall\, y \\ u = 1 \quad \theta = e^{-t} \quad C = e^{-t} \quad \text{for} \quad t > 0 \quad \text{and} \quad y = 0 \\ u = 0 \quad \theta \to 0 \quad C \to 0 \quad \text{for} \quad y \to \infty. \end{gathered} \tag{13}$$

The degree of practical attention include the Skin friction coefficients C_f, local Nusselt Nu, and local Sherwood Sh numbers are known as follows:

$$\begin{aligned} C_f &= -\left(1 + \frac{1}{\beta}\right) \left(\frac{\partial u}{\partial y}\right)_{y=0} \\ Nu &= -\left(\frac{\partial \theta}{\partial y}\right)_{y=0} \\ Sh &= -\left(\frac{\partial C}{\partial y}\right)_{y=0} \end{aligned} \tag{14}$$

3. Numerical Method of Solution

The nonlinear governing Eqs (10-12) along with the associated initial and boundary conditions (13) are solved numerically via Crank-Nicolson implicit finite difference method.The Crank-Nicolosn method is unconditionally stable and of second-order accuracy in both spatial $\left(o\left(\Delta y^2\right)\right)$ and temporal $\left(o\left(\Delta t^2\right)\right)$ directions.The Calculation

is executed for $\Delta y = 0.1$, $\Delta t = 0.001$ and procedure is repeated till $y = 4$. the velocity equation (10), the energy equation (11)and the equation of conservation of species (12) are written in their transient forms since procedure of the Cranck Nicolson implicit finite difference method is performed.

$$\begin{aligned}
&\frac{u_{i,j+1} - u_{i,j}}{\Delta t} - \frac{u_{i+1,j} - u_{i,j}}{\Delta y} \\
&= \left(1 + \frac{1}{\beta}\right)\left(\frac{u_{i-1,j} - 2u_{i,j} + u_{i-1,j} - 2u_{i,j+1} + u_{i+1,j+1}}{2(\Delta y)^2}\right) \\
&+ Gr\left(\frac{\theta_{i,j+1} - \theta_{i,j}}{2}\right) + Gm\left(\frac{C_{i,j+1} - C_{i,j}}{2}\right) - \left(M + \frac{1}{K}\right)\left(\frac{u_{i,j+1} + u_{i,j}}{2}\right)
\end{aligned} \tag{15}$$

$$\begin{aligned}
&\frac{\theta_{i,j+1} - \theta_{i,j}}{\Delta t} - \frac{\theta_{i+1,j} - \theta_{i,j}}{\Delta y} \\
&= \frac{1}{Pr}\left(1 + \frac{4R}{3}\right)\left(\frac{\theta_{i-1,j} - 2\theta_{i,j} + \theta_{i-1,j} - 2\theta_{i,j+1} + \theta_{i+1,j+1}}{2(\Delta y)^2}\right) \\
&+ Du\left(\frac{C_{i-1,j} - 2C_{i,j} + C_{i-1,j} - 2C_{i,j+1} + C_{i+1,j+1}}{2(\Delta y)^2}\right) - Q\left(\frac{\theta_{i,j+1} - \theta_{i,j}}{2}\right)
\end{aligned} \tag{16}$$

$$\begin{aligned}
&\frac{C_{i,j+1} - C_{i,j}}{\Delta t} - \frac{C_{i+1,j} - C_{i,j}}{\Delta y} \\
&= \frac{1}{Sc}\left(\frac{C_{i-1,j} - 2C_{i,j} + C_{i-1,j} - 2C_{i,j+1} + C_{i+1,j+1}}{2(\Delta y)^2}\right) \\
&+ Sr\left(\frac{\theta_{i-1,j} - 2\theta_{i,j} + \theta_{i-1,j} - 2\theta_{i,j+1} + \theta_{i+1,j+1}}{2(\Delta y)^2}\right) - K_r\left(\frac{C_{i,j+1} + C_{i,j}}{n}\right)^2
\end{aligned} \tag{17}$$

and transient form of initial and boundary conditions are:

$$\begin{aligned}
&u_{i,0} = 0 \quad \theta_{i,0} = 0 \quad C_{i,0} = 0 \quad \text{for all} \quad i = 1, 2, 3 \ldots \\
&u_{0,j} = 1 \quad \theta_{0,j} = e^{-j\Delta t} \quad C_{0,j} = e^{-j\Delta t} \quad \text{for all} \quad j = 1, 2, 3 \ldots \\
&u_{n,j} = 0 \quad \theta_{n,j} \to 0 \quad C_{n,j} \to 0
\end{aligned} \tag{18}$$

where index i and j are represents in spatial direction y temporal direction t, $\Delta y = y_{i+1} - y_i$ and $\Delta t = t_{j+1} - t_j$. To find the values of u, θ and C at time t, we may compute the values at time $t + \Delta t$ applying the following procedure: we substitute $i = 1, 2, ..., N-1$, where N correspond to ∞, equations (15) to (17) give tridiagonal system of equations with boundary conditions in equation (18), are solved employing Thomos algorithm as discussed in Carnahan et al.[13], we find values of θ and C for all values of y at $t + \Delta t$. Equation (15) is solved by same to substitute these values of θ and C, we get solution for u till desired time t.

4. Result and Discussion

In this section of article, numerically calculated consequences are showed off graphically and numerically. For the proper values of these parameters Dufour number $Du = 0.2$, Chemical reaction parameter $Kr = 1.2$, heat

source/sink parameter $Q = 2$, Schmidt number $Sc = 0.6$, Soret number $Sr = 1.5$, order of chemical reaction $n = 2$, radiation parameter $R = 2.2$, magnetic parameter $M = 4.8$, Casson $\beta = 0.4$, $t = 0.2$, $Gr = 4$, $Gm = 7$, $K = 1.5$ and $Pr = 0.7$ are kept constant through out the calculation unless otherwise stated in the respective graphs and tables.

Figures (1) and (2) show the impact of chemical reaction parameter Kr, in figure (1) velocity profile decreases slowly near to plate while concentration profile in figure (2) decreases near to plate after towards free stream concentration profile incerases. It is important that there is negligible change in temperature profile on increasing Schmidt number Sc in figure (3). Figure (4) depicts that boundary layer of concentration decreases rapidly when Schmidt number Sc increases.

Figures (5-7) show the influence of radiation parameter R on velocity profile, temperature profile and concentration profile respectively. It is observed that velocity profile and temperature profile increases in figures (5) and (6) respectively while concentration profile decreases near to plate after then increases in figure (7) on increasing radiation parameter R. The negative value of $Q < 0$ means heat absorption and the positive value of $Q > 0$ means heat transfer. In figure (8), velocity profile decreases on increasing heat source/sink parameter Q and also reducing momentum boundary layer. Figure (9) analyzed the impact of heat source/sink parameter Q in the temperature profile. It can be seen that the temperature profile decreases rapidly and the thermal boundary layer reduces for an increase of heat source parameter but it increases with the heat sink parameter. Figure (10) depicts that concentration profile increases near to plate from middle of boundary layer it decreases as well as species boundary layer reduces on an increase of heat source/sink parameter. Figures (11-13) show the change of dufour number Du. It is analyzed that velocity profile increases in figure (11) middle of momentum boundary, the temperature profile in figure (12) increases and concentration profile in figure (13) decreases on increasing Dufour number Du.

Figure (14) shows the effect of Casson fluid parameter β on velocity profile. It is observed that velocity increase near to plate after then decreases as well as momentum boundary layer reduces on increasing Casson fluid parameter. Figures (15-17) and (18-20) plot the effect of Soret number Sr and time t respectively on velocity profile, temperature profile and concentration profile. Velocity profile, temperature profile, concentration profile, and corresponding boundary layers also increase on increasing Soret numbers Sr and time t. Velocity profile decreases and reduces boundary layer thickness in figure 21 on an increase of Schmidt number Sc.

Table 1 provides change of Skin friction coefficient C_f, Nusselt number Nu and Sherwood number Sh. It is seen that the Skin friction coefficient increases on an increase of chemical reaction parameter Kr, heat source/sink parameter Q and Schmidt number Sc on the other hand it decreases on an increase of Dufour number Du, radiation parameter R, Soret number Sr, Casson fluid parameter β and time t. Nusselt number Nu increases on increase heat source/sink parameter Q and Soret number Sr and decreases on increase Dufour number Du, chemical reaction parameter Kr, radiation parameter R, Schmidt number Sc and time t. Sherwood number increases on increase Dufour number Du, chemical reaction parameter Kr, radiation parameter R, Schmidt number Sc and time t and decreases on increase heat source/sink parameter Q and Soret number Sr.

5. Conclusion

This research work presents the unsteady MHD Casson fluid flow over a porous plate with the Soret-Dufour effect, higher-order chemical reaction, thermal radiation, and heat source-sink that emerged in a porous medium. The governing partial differential equations are transformed into nondimensional partial differential equations using similarity transformation, which are solved using Crank-Nicolson implicit finite difference method. The

results for velocity, temperature, and concentration are shown graphically and the Skin friction coefficient, Nusselt number, and Sherwood number are shown in the table.
The prime observation of this investigation are remarked as:

1. The fluid velocity increases near to plate after then it decreases and momentum boundary layer reduces on an increase of Casson fluid parameter β.
2. On the increase of Soret number Sr, thermal boundary layer reduces.
3. On the increase of Dufour number Du, species boundary layer reduces.
4. On the increase of heat source/sink parameter Q momentum, thermal and species boundary layer increases.
5. On the increase of heat source/sink parameter Q, concentration near to plate increases after then decreases.
6. On the increase of chemical reaction parameter Kr, species boundary layer increases.

Figure 1. Velocity Profiles for Different Values of Kr

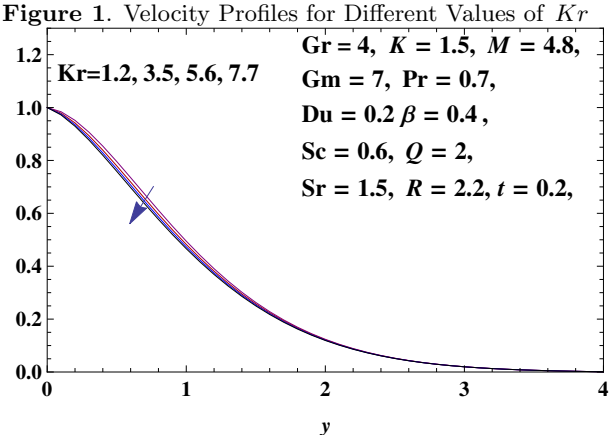

Figure 2. Concentration Profiles for Different Values of Kr

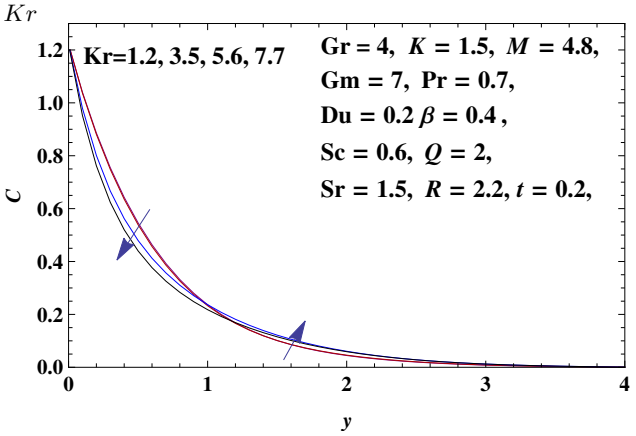

Figure 3. Temperature Profiles for Different Values of Sc

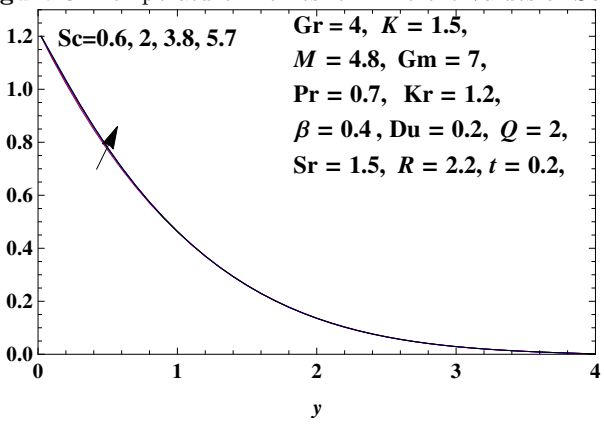

Figure 4. Concentration Profiles for Different Values of Sc

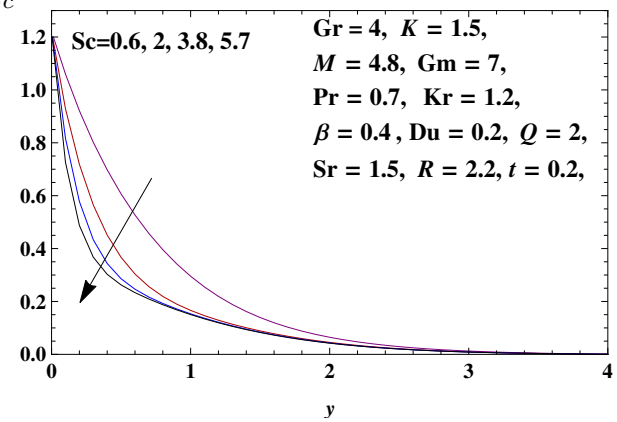

Figure 5. Velocity Profiles for Different Values of R

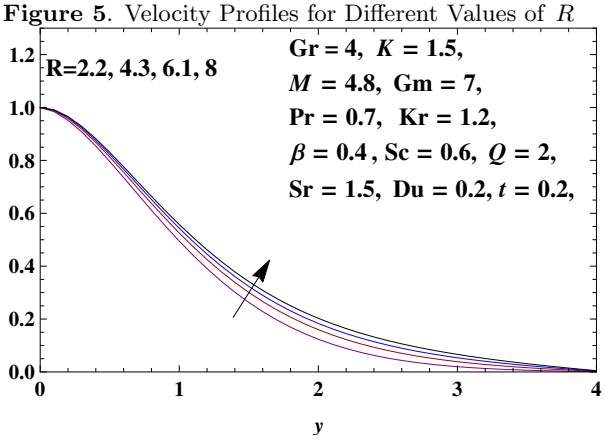

Figure 6. Temperature Profiles for Different Values of R

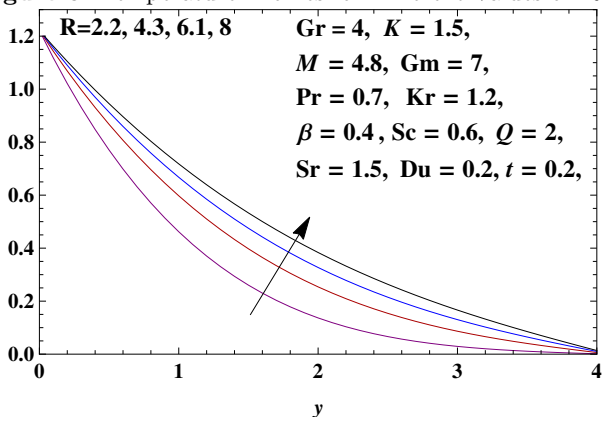

Figure 7. Concentration Profiles for Different Values of R

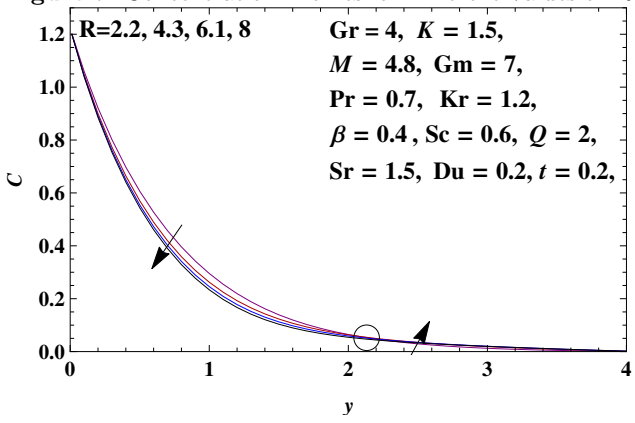

Figure 8. Velocity Profiles for Different Values of Q

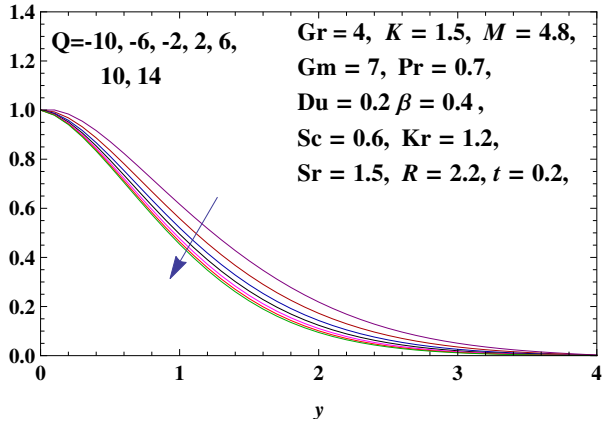

Figure 9. Temperature Profiles for Different Values of Q

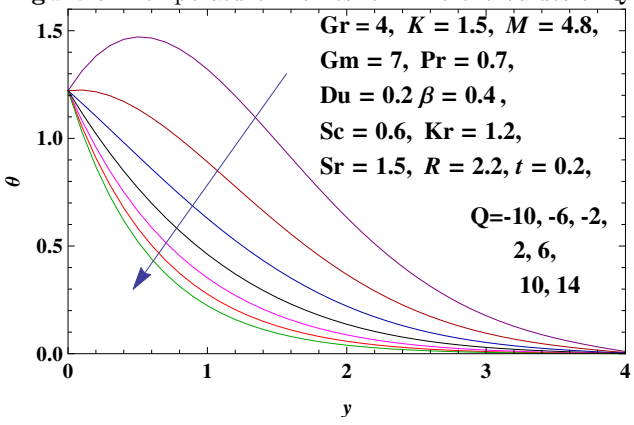

Figure 10. Concentration Profiles for Different Values of Q

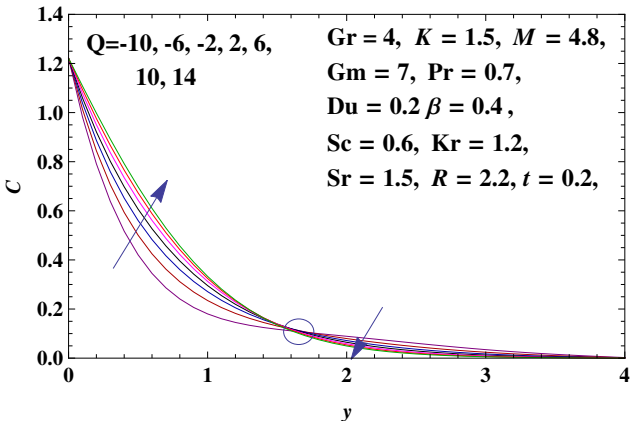

Figure 11. Velocity Profiles for Different Values of Du

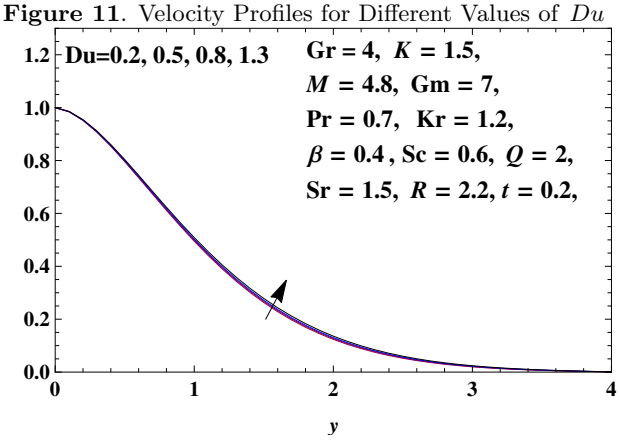

Figure 12. Temperature Profiles for Different Values of Du

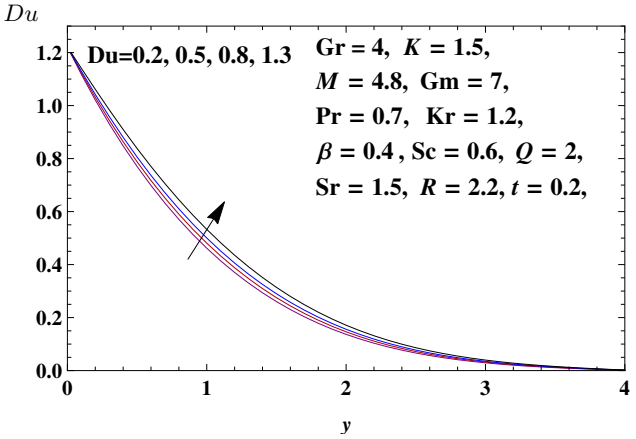

Figure 13. Concentration Profiles for Different Values of Du

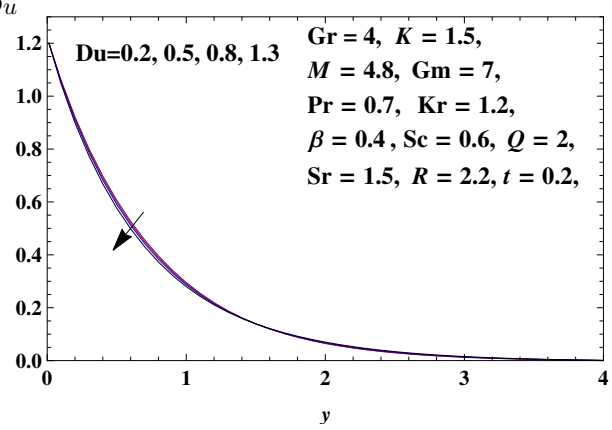

Figure 14. Velocity Profiles for Different Values of β

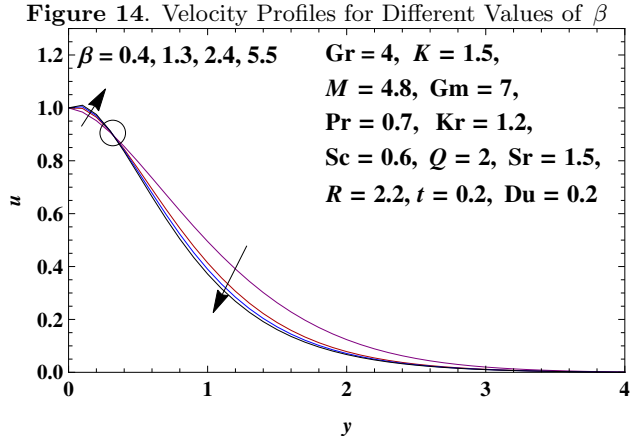

Figure 15. Velocity Profiles for Different Values of Sr

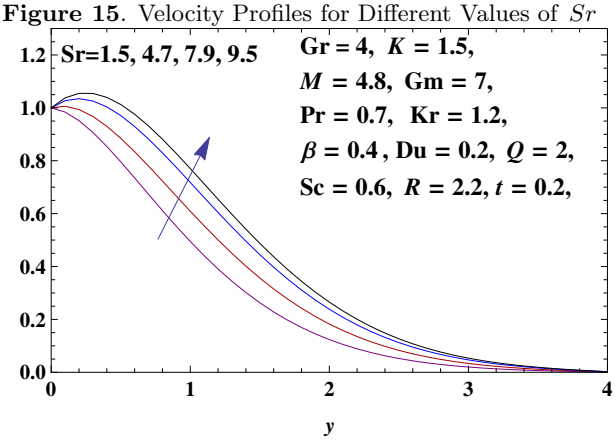

Figure 16. Temperature Profiles for Different Values of Sr

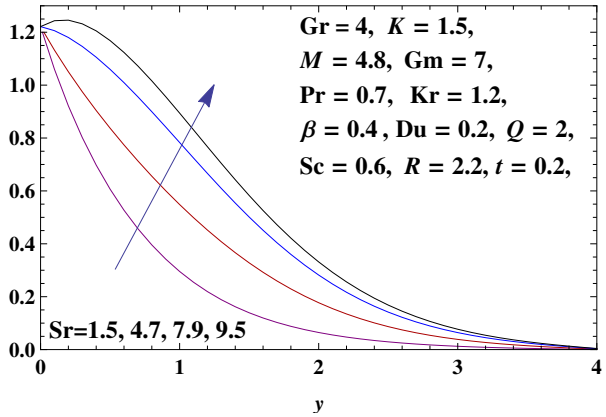

Figure 17. Concentration Profiles for Different Values of Sr

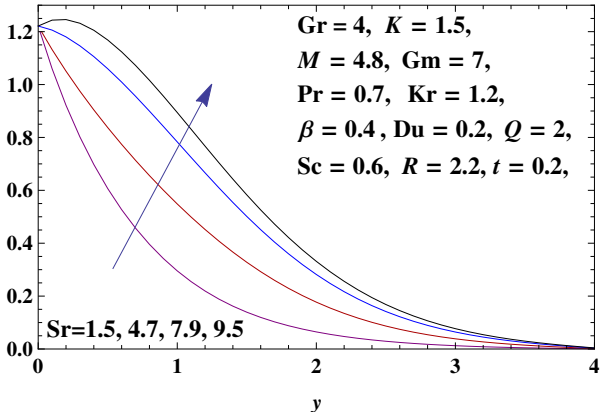

Figure 18. Velocity Profiles for Different Values of t

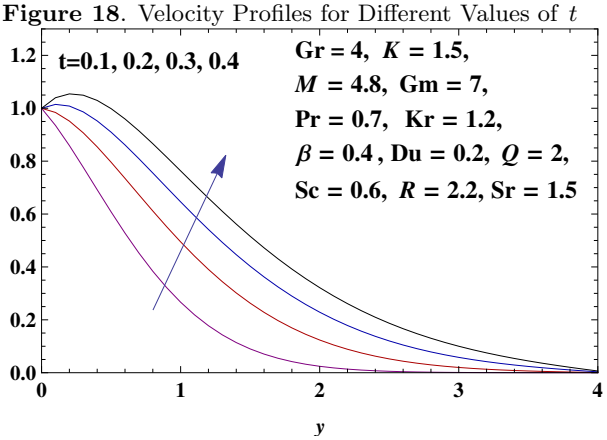

Figure 19. Temperature Profiles for Different Values of t

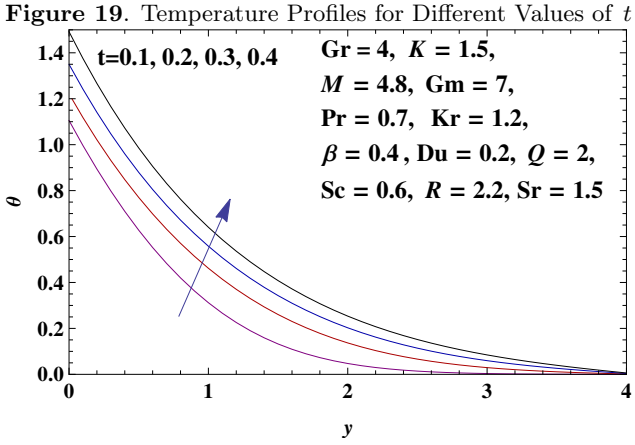

Figure 20. Concentration Profiles for Different Values of t

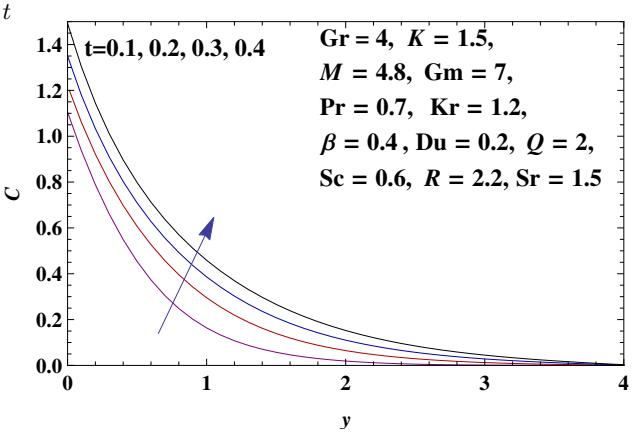

Figure 21. Velocity Profiles for Different Values of Sc

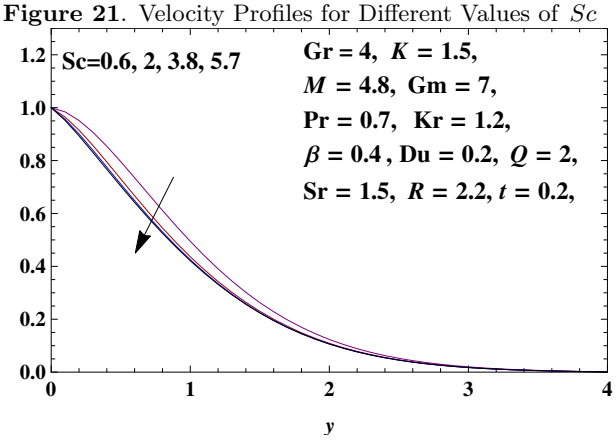

Table 1. Skin friction coefficient C_f, Nusselt number Nu and Sherwood number Sh for different values of parameters taking fix values of $Gr = 4, Gm = 7, K = 1.5, M = 4.8, n = 2, Pr = 0.7$

Du	Kr	Q	R	Sc	Sr	β	t	C_f	Nu	Sh
0.2	1.2	2	2.2	0.6	1.5	0.4	0.2	0.556363	1.036	1.61551
0.5	1.2	2	2.2	0.6	1.5	0.4	0.2	0.541777	0.978101	1.64983
0.8	1.2	2	2.2	0.6	1.5	0.4	0.2	0.527095	0.916485	1.68687
1.3	1.2	2	2.2	0.6	1.5	0.4	0.2	0.502426	0.804171	1.75567
0.2	3.5	2	2.2	0.6	1.5	0.4	0.2	0.743168	1.02108	2.08997
0.2	5.6	2	2.2	0.6	1.5	0.4	0.2	0.874172	1.01044	2.42351
0.2	7.7	2	2.2	0.6	1.5	0.4	0.2	0.980252	1.00164	2.6963
0.2	1.2	−10	2.2	0.6	1.5	0.4	0.2	−0.0167	−0.915942	2.38844
0.2	1.2	−6	2.2	0.6	1.5	0.4	0.2	0.258115	−0.0318611	2.07768
0.2	1.2	−2	2.2	0.6	1.5	0.4	0.2	0.436688	0.582744	1.82613
0.2	1.2	6	2.2	0.6	1.5	0.4	0.2	0.639071	1.38849	1.43426
0.2	1.2	10	2.2	0.6	1.5	0.4	0.2	0.697964	1.67519	1.27483
0.2	1.2	14	2.2	0.6	1.5	0.4	0.2	0.741101	1.91694	1.13214
0.2	1.2	2	4.3	0.6	1.5	0.4	0.2	0.433918	0.783753	1.73754
0.2	1.2	2	6.1	0.6	1.5	0.4	0.2	0.362143	0.670918	1.78681
0.2	1.2	2	8	0.6	1.5	0.4	0.2	0.305201	0.594307	1.81858
0.2	1.2	2	2.2	2	1.5	0.4	0.2	1.24005	0.993209	2.92713
0.2	1.2	2	2.2	3.8	1.5	0.4	0.2	1.53342	0.955427	4.04132
0.2	1.2	2	2.2	5.7	1.5	0.4	0.2	1.68956	0.924276	4.94899
0.2	1.2	2	2.2	0.6	4.7	0.4	0.2	−0.208112	1.05736	0.892239
0.2	1.2	2	2.2	0.6	7.9	0.4	0.2	−0.952718	1.07961	0.155016
0.2	1.2	2	2.2	0.6	9.5	0.4	0.2	−1.31898	1.09115	−0.222022
0.2	1.2	2	2.2	0.6	1.5	1.3	0.2	0.0354141	1.036	1.61551
0.2	1.2	2	2.2	0.6	1.5	2.4	0.2	−0.0603321	1.036	1.61551
0.2	1.2	2	2.2	0.6	1.5	5.5	0.2	−0.118269	1.036	1.61551
0.2	1.2	2	2.2	0.6	1.5	0.4	0.1	2.27056	1.08151	1.69254
0.2	1.2	2	2.2	0.6	1.5	0.4	0.3	−0.512663	1.08359	1.71789
0.2	1.2	2	2.2	0.6	1.5	0.4	0.4	−1.39326	1.1672	1.89457

References

[1] Shaw S. and Mahantha G. 3D Casson fluid flow past a porous linearly stretching sheet with convective boundary conditions. Alexandria Engineering Journal, 2015; 54(3), 653–659.

[2] Hayat T., Eid M. R., Alsaedi A. and Muhammad T. Comprehensive analysis of heat transfer of gold-blood nanofluid (Sisko-model) with thermal radiation. Results in Physics, 2017; 7, 4388–4393.

[3] Eid M. R., Ibrahim F. S., Hady F. M. and Abdel-Gaied S. M. Radiation effect on viscous flow of a nanofluid and heat transfer over a nonlinearly stretching sheet. Nanoscale Research Letters, 2012; 7(1), 229.

[4] Islam S., Khan N.S., Zuhra S., Bonyah E., Khan M.A. and Khan W. Flow and heat transfer in water based liquid flm fuids dispensed with graphene nanoparticles. Res Phys., 2018; 8, 1143–1157.

[5] Sandeep N., Sugunamma V., Ramadevi B., Anantha Kumar K., Reddy J.V.R. Magnetohydrodynamic mixed convective fow of micropolar fuid past a stretching surface using modifed Fourier's heat fux model. J Thermal Anal Calorim. 2019.

[6] Shehzad S.A., Hayat T., Qayyum S. and Alsaedi A. Efect of a chemical reaction on magnetohydrodynamic (MHD) stagnation point fow of Walters-B nanofuid with newtonian heat and mass conditions. Nucl Eng Technol., 2017; 49, 1636–1644.

[7] Afify A.A. The influence of slip boundary condition on Casson nanofluid flow over a stretching sheet in the presence of viscous dissipation and chemical reaction. Mathematical Problems in Engineering. 2017; Article ID 3804751, 12 pages, 2017. https://doi.org/10.1155/2017/3804751.

[8] Hammad Alotaibi, Saeed Althubiti, Mohamed R. Eid, and Mahny K. L. Numerical Treatment of MHD Flow of Casson Nanofluid via Convectively Heated Non-Linear Extending Surface with Viscous Dissipation and Suction/Injection Effects. Computers, Materials & Continua, 2021; 66(1), 229–245.

[9] Kirubhashankar C. K., Vaithyasubramanian S., Immanuel Y. and Muniappan P. Thermal Effects on Magneto Hydrodynamic Casson Liquid Stream Between Electrically Conducting Plates. International Journal of Innovative Technology and Exploring Engineering., 2020; 9(4), 213–217.

[10] Amos S. Idowu, Mojeed T. Akolade, Jos U. Abubakar and Bidemi O. Falodun MHD free convective heat and mass transfer flow of dissipative Casson fluid with variable viscosity and thermal conductivity effects. JOURNAL OF TAIBAH UNIVERSITY FOR SCIENCE., 2020; 14(1), 851–862.

[11] Bhuvaneswari, M., Eswaramoorthi, S., Sivasankaran, S. and Hussein, A.K. Cross-diffusion effects on MHD mixed convection over a stretching surface in a porous medium with chemical reaction and convective condition, Engineering Transactions, 2019; 67(1), 3–19.

[12] Mansour, M., Rashad, A., Mallikarjuna, B., Hussein, A.K., Aichouni, M. and Kolsi, L. MHD mixed bioconvection in a square porous cavity filled by gyrotactic microorganisms, International Journal of Heat and Technology, 2019; 37(2), 433–445.

[13] Brice Carnahan, Luther H.A. and James O. Wilkes., Applied Numerical Methods, Krieger Pub Co, Florida, 1990.